Int. J. Multiphase Flow Vol. 10, No. 1, pp. 21–40, 1984
Printed in Great Britain.

0301-9322/84 $3.00 + .00
Pergamon/Elsevier

A MECHANISTIC NON-EQUILIBRIUM MODEL FOR TWO-PHASE CRITICAL FLOW

E. ELIAS†

S. Levy, Inc., 1999 South Bascom Avenue, Campbell, CA 95008, U.S.A.

and

P. L. CHAMBRÉ

Department of Nuclear Engineering, University of California, Berkeley, CA 94720, U.S.A.

(*Received* 27 *June* 1982; *in revised form* 11 *April* 1983)

Abstract—A one-dimensional mechanistic model is developed to calculate the critical mass flux of an initially two-phase, saturated or subcooled fluid. A new formulation is incorporated to account for bubble formation, growth and convection. The model allows for thermal non-equilibrium vapor drift velocity and non-uniform bubble distribution.

The model has been qualified in comparison with available critical flow data for water in horizontal and vertical discharge pipes and converging-diverging nozzles. Predictions compare favorably with experimental data over a wide range of pressures and pipe diameters and lengths.

1. INTRODUCTION

Two-phase flow of vapor and superheated liquid exists during blowdown of a two-phase vapor–liquid mixture or of an initially saturated or subcooled liquid. An understanding of the physics governing the two-phase flow of one-component superheated liquids is useful in the design of boilers, refrigeration and desalinization equipments and in the handling of liquified gases. Much of the progress in modeling superheated flows has been derived from the need to predict critical flow rates in the blowdown safety analysis of water cooled nuclear reactors.

The flow of a superheated liquid is basically a metastable process. Studies of superheated flashing flows are, therefore, directed towards the determination of the vapor generation rate as the system relaxes from its excited or thermodynamic non-equilibrium state to equilibrium. This relaxation is typically carried out by heat diffusion and evaporation processes.

Over the past two decades there have been many theoretical and experimental studies of non-equilibrium flashing flow. The main aspects of the problem related to critical flow are discussed in several review articles by Boure (1977), Jones & Saha (1977), Ardron & Furness (1976) and Wallis (1980). A comprehensive review and discussion of analytical models and key experimental results in the area of two-phase critical flow has been compiled by Abdollahian *et al.* (1980, 1982), with about 250 references cited. It has generally been found that phase equilibrium blowdown models are not valid for discharge from short pipes or nozzles. For such geometries the two-phase expansion is too rapid for the two phases to reach equilibrium. Temperature and pressure measurements indicated substantial liquid superheat during blowdown from short nozzles. Furthermore, the vapor and liquid phases typically attain different velocities. These observations call for the development of a non-homogeneous and non-equilibrium model to predict the experimental data.

Non-equilibrium models are generally divided into empirical methods (Henry *et al.* 1970; Henry 1980; Simpson & Silver 1962) and mechanistic models (Edwards 1968; Winters & Merte 1979; Malnes 1975; Ardron 1978). The first approach accounts for non-equilibrium vapor generation by introducing one or more empirical coefficients to keep the flow quality below its equilibrium value. The coefficients are typically fitted to experimental data with no attempt to describe the mechanism of vapor formation. In the second approach, the problem is formulated from a mechanistic point of view. The vapor generation is generally modeled as a bubble

†On leave from the Department of Nuclear Engineering, Technion–Haifa, Israel.

growth process following Plesset & Zwick (1954) or Forster & Zuber (1954). It is assumed that the rate of growth is governed by transient conduction in the liquid surrounding each bubble with no effects from neighboring bubbles.

Incorporating a bubble growth model in the analysis of superheated liquid flow requires simultaneous solution of the fluid field equations in conjunction with constitutive relations to account for bubble convection, growth and interfacial energy transfer. Various approximations are typically made to simplify these equations. Winters & Merte (1979) used a lumped parameter approach and neglected the effect of relative velocity and bubble convection. Ardron (1978) approximated the spatial variation of the temperature difference across the bubble surface by an arbitrary linear function and thus omitted the energy conservation equation. The one-dimensional two-fluid equations for the conservation of mass and momentum were then solved numerically to predict the critical flow data assuming the liquid temperature is constant. While it is demonstrated that the above models are successful in predicting critical flow data for initially subcooled or saturated conditions, the effect of the various approximations made in deriving the vapor phase equation on the predicted critical mass flux is not fully elaborated.

This paper develops a mechanistic model for non-equilibrium critical flow of an initially two-phase, saturated or subcooled liquid. The model is based on a one-dimensional drift flux formulation of the mass, momentum and energy field equations of the two-phase mixture and incorporates a new formulation of the vapor phase equation. It allows for interphase liquid–vapor relative motion, thermal non-equilibrium wall heat flux and radial non-uniform distribution of bubbles. Predictions of the new model are compared with available data for steady critical flow in nozzles, pipes and converging–diverging test sections. The effect of the pipe length and reservoir stagnation conditions on the critical flow rate is analyzed. The predicted critical mass flux for long flow channels are typically lower than the homogeneous equilibrium prediction due to wall friction. Predictions for short discharge pipes are shown to be affected by thermal non-equilibrium in the flow and lie above the predictions which are based on the homogeneous equilibrium approximation.

2. CONSERVATION EQUATION

Basically we establish a four-equation model: three mixture balance equations and one phase mass balance. This set is closed if two restrictions are imposed. We assume: (1) vapor is at saturation temperature corresponding to the imposed liquid pressure and (2) a drift velocity is given as a function of physical properties. The remaining dependent variables are the vapor void fraction, pressure, liquid enthalpy and mixture mass flux.

2.1 *Mixture equations*

The mixture conservation equations used are based on the one dimensional drift flux model (Lahey & Moody 1977; Dobran 1981). For steady-state conditions the two-phase mixture mass equation is:

$$\frac{\mathrm{d}}{\mathrm{d}z}(GA) = 0. \qquad [1]$$

The steady-state momentum equation is given by:

$$\frac{1}{A}\frac{\mathrm{d}}{\mathrm{d}z}\left(\frac{AG^2}{\bar{\rho}}\right) + \frac{2fG^2}{\bar{\rho}D} + \bar{\rho}g\cos\theta' + \frac{1}{A}\frac{\mathrm{d}}{\mathrm{d}z}\left(A\frac{\alpha}{1-\alpha}\frac{\rho_L\rho_G}{\bar{\rho}}V_{Gj}'^2\right) = -\frac{\mathrm{d}P}{\mathrm{d}z} - \left(\frac{\mathrm{d}P}{\mathrm{d}z}\right)_{\text{loc.}} \qquad [2]$$

where ρ_L, ρ_G and $\bar{\rho}$ denote respectively the liquid, vapor and mixture density. α is the vapor volumetric concentration, G is the mixture mass flux, V_{Gj}' is the drift velocity of the vapor phase with respect to the center of volume, f is a friction coefficient, D and A are the local duct hydraulic diameter and flow area and θ' is the duct inclination angle. P is the pressure at position z, g is the acceleration due to gravity and the subscript loc. denotes local property.

Equation [2] is written in Eulerian form in terms of the center-of-mass of the two phase mixture and incorporates the conventional simplifying assumptions that some of the averages of products of dependent variable across the duct are identical to products of averages. Momentum transfer due to turbulence is neglected. The last term on the left hand side of [2] is due to the relative velocity between the phases. It represents the net momentum flux with respect to the center of mass of the flowing two phase mixture. Local irreversible pressure loss associated with an abrupt area change is accounted for in the last term on the r.h.s. of [2].

The steady-state mixture energy equation for non-equilibrium two-phase flow is:

$$G\frac{dH}{dz}+\frac{1}{A}\frac{d}{dz}\left(A\alpha\frac{\rho_G\rho_L}{\bar{\rho}}V'_{Gj}h_{LG}\right)=\left\{\frac{G}{\bar{\rho}}+\frac{1}{\bar{\rho}}(\rho_L-\rho_G)\alpha V'_{Gj}\right\}\frac{dP}{dz}+\frac{q''P_H}{A}. \quad [3]$$

Here H is the specific enthalpy of the two-phase mixture and h_{LG} is the latent heat. In [3] we have neglected the effects of frictional heating and change of kinetic energy due to the relative velocity between vapor and liquid. Equation [3] is written for non-homogeneous flow and allows for heat flux q'' from a heated boundary surface of perimeter P_H. The second term on the l.h.s. of [3] represents the drift of energy through the center of mass plane of the two phase mixture.

2.2 *Vapor phase equation*

Assuming that the vapor density is uniform over the flow cross-section, the steady state equation of conservation of mass of the vapor phase is:

$$\frac{d}{dz}(Au_G\alpha\rho_G)=\Gamma_G \quad [4]$$

where u_G is the vapor phase velocity averaged over the phase volume and Γ_G is the mass of liquid evaporated per unit time and length of the flow path. The magnitude of this evaporation term depends on the transient and thermodynamic conditions in the flow, which are in turn a function of position z.

3. CONSTITUTIVE AND STATE RELATIONS

Equations [1]–[4] form a complete set of field equations. To close the model requires a set of constitutive and state relations to describe the fluid mixture properties and the exchange of momentum and energy between the fluid mixture and the bounding surfaces. This section describes the relations for the wall friction coefficient, f, local irreversible pressure drop $\Delta P_{loc.}$, drift velocity V'_{Gj}, wall heat flux and thermodynamic and transport properties of vapor and liquid. A relation for the vapor formation rate Γ_G, is developed separately in the following section.

3.1 *Pressure drop and heat flux*

For turbulent flow, which is the condition most usually of interest here, a suitable empirical relation for f is (Streeter 1961):

$$\frac{1}{\sqrt{f}}=3.48+4\log(D/9\times10^{-5}). \quad [5]$$

The general local irreversible pressure drop equation is similar to that for friction pressure drop:

$$\Delta P_{loc.}=K\frac{G^2}{2\bar{\rho}} \quad [6]$$

where the single phase form loss coefficient, K is determined from handbooks of hydraulic resistances, (e.g. Streeter 1961).

Since no data is currently available on the effect of wall heat flux on the critical two-phase flow, the wall heat flux term in [3] was set equal to zero.

3.2 *Drift velocity*

The vapor drift velocity is expressed in terms of the void-weighted average velocity of the vapor phase (Lahey & Moody 1977):

$$V'_{Gj} = \frac{\bar{\rho}}{\rho_L}\left(u_G - \frac{G}{\bar{\rho}}\right) = \frac{\bar{\rho}V_{Gj} + (C_0 - 1)G}{\bar{\rho} - (C_0 - 1)(\rho_L - \rho_G)\alpha} \tag{7}$$

where C_0 is a concentration parameter which quantifies the effect of the radial distribution of void and V_{Gj} is the void weighted vapor drift velocity with respect to the center of volume of the two-phase mixture.

For flow in a horizontal pipe V_{Gj} was set equal to zero. For vertical flow the drift velocity was calculated by (Lahey & Moody 1977):

$$V_{Gj} = 1.41\left[\frac{\sigma g(\rho_L - \rho_G)}{\rho_L^2}\right]^{1/4} \cos\theta' \tag{8}$$

where σ is surface tension and $\cos\theta' = 1$ for liquid upflow and $\cos\theta' = -1$ for liquid downflow. Equation [8] is strictly applicable for equilibrium bubbly flow. This equation is used here since no better expression is currently available for non-equilibrium situations.

3.3 *State equations*

The state equation for steam and water was obtained from analytical fits to steam table data and are accurate to within a few percentage points for the pressure and temperature ranges of interest. To simplify the computation procedure it was assumed that the vapor is an ideal gas which obeys the saturated vapor pressure law obtained by the Clausius–Clapeyron equation:

$$\frac{d\rho_G}{dP} = \frac{\rho_G}{P} - \frac{1}{h_{LG}} \tag{9}$$

4. EVAPORATION RATE

To determine the evaporation rate term Γ_G we consider the growth in the superheated liquid of vapor bubbles of radius r. The determination of r requires the simultaneous solution of the equations for the vapor pressure in the bubble, the time dependent thermal conduction in the liquid layer surrounding the bubble and the dynamics of the bubble. A number of approximate solutions available in the literature greatly simplify the analysis. Since in the following the bubble population is averaged over the flow cross section, the influence of the wall on the bubble radius history is ignored. In addition, convection heat transfer is insignificant for small bubble size and low relative velocity. The bubble radius is, therefore, determined by a conduction bubble growth model (Forster & Zuber 1954).

$$r = 2k\left(\frac{\sqrt{(\lambda_p C_p)_L}}{h_{LG}\rho_G}\right)(T_L - T_s)\sqrt{t},\ k = \sqrt{\frac{3}{\pi}}. \tag{10}$$

Here T_L is the temperature of the liquid surrounding the bubble and T_s is the vapor temperature taken to be at saturation, λ and C_p are the liquid conductivity and specific heat respectively. In

a steady temperature and pressure field [10] can be restated as:

$$\frac{dr}{dt} = \beta^2 \frac{(T_L - T_s)^2}{r}, \beta = k \frac{\sqrt{2(\lambda_\rho C_p)_L}}{h_{LG}\rho_G}. \quad [11]$$

The principal assumption is now made that the rate law [11] is valid also in an element of the vapor phase which travel with the speed of the vapor. Equation [11] can be stated in the Lagrangian view as

$$\frac{Dr}{Dt} = \beta^2 \frac{(T_L - T_s)^2}{r} \quad [12]$$

where Dr/Dt is a substantial derivative.

In order to arrive at a constitutive relation for the vapor rate of formation, a concentration N is defined as the number of bubbles of radius r lying between r and $r + dr$, per unit volume of fluid and vapor mixture, per unit radius difference dr. The number of bubbles whose radii lie between r to $r + dr$ is therefore $N\,dr$, per unit volume of fluid and vapor mixture. In a short time interval dt a bubble which did lie inside the range $r - dr$ to $r - dr + (Dr/Dt)\,dt$ will pass into the range r to $r + dr$. Similarly, a bubble which was located inside the range r to $r + [(Dr/Dt) + d(Dr/Dt)]\,dt$ will leave the range $r + dr$. The reason for including the term $d(Dr/Dt)$ is that Dr/Dt is a function of r as seen by [12] and Dr/Dt is considered in neighboring r intervals. Hence, the increase in the number of bubbles in the range dr and time dt is in view of these considerations, and the definition of N,

$$-dN\,dr = \left\{(N + dN)\left[\frac{Dr}{Dt} + d\left(\frac{Dr}{Dt}\right)\right] - N\frac{Dr}{Dt}\right\} dt = \left\{dN\frac{Dr}{Dt} + N\,d\left(\frac{Dr}{Dt}\right)\right\} dt$$

which is correct to first order of the differential terms. Hence, on division by dt and dr and combining the terms on the r.h.s:

$$-\left(\frac{\partial N}{\partial t}\right)_{\text{growth}} = \frac{\partial}{\partial r}\left(N\frac{Dr}{Dt}\right) \quad [13]$$

$(\partial N/\partial t)_{\text{growth}}$ represents the bubble concentration growth rate of bubbles of radius r lying between r and $r + dr$ per unit volume of fluid and vapor mixture, per unit radius difference dr. Under steady-state conditions the rate of change of bubble density due to growth is balanced by convection, yielding

$$\left(\frac{\partial N}{\partial t}\right)_{\text{growth}} = \frac{1}{A}\frac{\partial}{\partial z}(N\,\text{Au}_G). \quad [14]$$

In this balance one observed that $(\partial N/\partial t)_{\text{growth}}$ is the growth rate per unit length in the flow direction. From [12] to [14] one obtains

$$\beta^2 \frac{\partial}{\partial r}\left[\frac{N}{r}(T_L - T_s)^2\right] + u_G \frac{\partial N}{\partial z} = -\frac{N}{A}\frac{\partial}{\partial z}(\text{Au}_G) \quad [15]$$

Defining, $(N/r) = n$, $1/2(r/\beta T_s)^2 = \tau$ and $[1 - (T_L(z)/T_s(z))]^2 = \phi(z)$, [15] becomes

$$\phi(z)\frac{\partial n}{\partial \tau} + u_G \frac{\partial n}{\partial z} = -\frac{n}{A}\frac{\partial}{\partial z}(\text{Au}_G). \quad [16]$$

Equation [16] is a new bubble species equation. Its solution describes the bubble number and

their radii distribution $n(z, \tau)$ along the flow channel. The function $\phi(z)$ describes the temperature field of the liquid–vapor mixture. It is directly related to the system pressure and liquid specific enthalpy. Therefore, a solution scheme should be considered in which [16] is solved along the flow channel in conjunction with the mixture and phase field equations. Such a scheme is described in this and the next sections.

The vapor generation rate Γ_G is now determined by integrating $(\partial N/\partial t)_{\text{growth}}$ over the range of bubble radii in the flow

$$\Gamma_G = \frac{4}{3}\pi\rho_G A \int_0^{R_\infty} \left(\frac{\partial N}{\partial t}\right)_{\text{growth}} r^3 \, dr \qquad [17]$$

where R_∞ is an arbitrary large bubble radius. Once n has been found from [16] one can determine $(\partial N/\partial t)_{\text{growth}}$ from [14] for the determination of $\Gamma_G(z)$.

Equations [14] and [17] must be considered together with the vapor phase equation [4]. It is [4] which determines the void fraction, α. By multiplying [14] with $4/3\pi\rho_G A r^3 \, dr$ and integrating with respect to r, one obtains with help of [17]

$$\Gamma_G = \frac{4}{3}\pi \frac{d}{dz}\left\{\rho_G A u_G \int_0^{R_\infty} n r^4 \, dr\right\}. \qquad [18]$$

A comparison with [4] then shows that the void fraction is

$$\alpha = \frac{4}{3}\pi \int_0^{R_\infty} n r^4 \, dr. \qquad [19]$$

It should be noted that [10] and [12] were originally derived to predict bubble growth at constant pressure. Their use in a variable pressure field along a flow path should therefore be considered as an approximation. The approximation is weakest mainly in region of rapidly changing pressure, e.g. near an orifice or at the choking plane in case of two phase critical flow. However, since the objective of the present calculations is to predict the location of the choking plane rather than its detailed structure, [10] and [12] are considered acceptable. Models for bubble growth in a variable pressure field (Jones & Zuber 1978; Cha & Henry 1981) can be incorporated in the evaporation rate model developed in this paper. This extension is presently under investigation.

4.1 *Solution by Laplace transformation*

Equation [16] is a first order nonhomogeneous hyperbolic equation which requires both "initial" conditions at $\tau = \tau_o$ and boundary conditions at $z = 0$, taken as the entrance to the flow section. In the general case of two-phase stagnation conditions we consider at the entrance to the flow channel an input of N bubbles per unit radius difference per unit volume with linearly distributed radii in the range r_0 to r_1, i.e.

$$N(r)\, dr = n_1 r \, dr \qquad [20]$$

For a given n_1, the maximum bubble radius (r_1 or τ_1) at the entrance can be determined by the known stagnation void fraction $\alpha(0)$ (i.e. [19]) and r_0

$$\alpha(0) = \frac{4}{3}\pi \int_{r_0}^{r_1} n_1 r^4 \, dr = \frac{4}{15}\pi n_1 (r_1^5 - r_0^5). \qquad [21]$$

A suitable boundary condition for $n(0, \tau)$ is therefore given by:

$$n(0, \tau) = \begin{cases} n_1, & \tau_0 \leq \tau \leq \tau_1 \\ 0, & \tau > \tau_1 \end{cases}. \quad [22]$$

Note that for subcooled or saturated entrance conditions [22] is reduced to

$$n(0, \tau) = 0, \ \tau > \tau_0. \quad [23]$$

Along the flow channel, foreign bodies and pipe surfaces normally provide ample nuclei for vapor formation. The number of vapor nuclei per unit volume of a two phase mixture per unit radius difference is described by:

$$n(z, \tau_o) = n_0[1 - \alpha(z)] \exp\left[\frac{-\psi \Delta G(z)}{k_b T_L(z)}\right] \quad [24]$$

which is comparable to the expression used for the embryo density in homogeneous nucleation.

In[24] k_b is the Boltzman constant, and n_0 is a constant describing the normalized number density of bubble nucleation sites in the liquid per unit radius difference. ΔG is the maximum free energy of bubble formation given by Cole (1979)

$$\Delta G(z) = \frac{16}{3} \frac{\pi \sigma^3}{[P(z) - P_s(T_L)]^2} \quad [25]$$

ψ is a factor which depends on the character of the cavities in the surface and the liquid contact angle. Typically $0 \leq \psi \leq 1$.

In [24] we assume that for the computation of n all vapor nuclei are formed with a uniform initial radius r_0 (or τ_0). It is important to note that the actual equilibrium nucleus radius depends on the local thermodynamic condition in the flow and in particular on the local liquid superheat.

The vapor species equation [16] can be written as

$$h(z) \frac{\partial n}{\partial t} + \frac{\partial n}{\partial z} = -ng(z) \quad [26]$$

where

$$t = \tau - \tau_0, \ h(z) = \phi(z)/u_G(z) \text{ and } g(z) = \frac{\mathrm{d}}{\mathrm{d}z} \ln(Au_G)$$

In terms of z and t the boundary and initial conditions are

$$n(z, 0) = n_0[1 - \alpha(z)] \exp\left(\frac{-\psi \Delta G(z)}{k_b T_L(z)}\right), \ z > 0$$

$$n(0, t) = n_1\{U(t) - U(t - t_1)\} \quad [27]$$

where $t_1 = \tau_1 - \tau_0$ and $U(t)$ is the unit step function. The Laplace transform of [26] with respect to t yields with the imposed initial condition

$$\frac{\mathrm{d}}{\mathrm{d}z} n(z, S) + [h(z)S + g(z)]n(z, S) = h(z)n(z, 0) \quad [28]$$

where

$$n(z, S) = \int_0^\infty \exp(-\mathrm{St}) n(z, t) \, \mathrm{d}t. \quad [29]$$

The general solution to this first order differential equation is

$$n(z, S) = C \exp\left\{-\int_0^z [h(z')S + g(z')]\,dz'\right\} + \exp\left\{-\int_0^z [Sh(z') + g(z')]\,dz'\right\}. \cdot \int_0^z \exp\left\{\int_0^{z'} [h(z'')S + g(z'')]\,dz''\right\}[h(z')n(z', 0)]\,dz'. \quad [30]$$

The constant of integration C can be evaluated using the Laplace transform of $n(0, t)$ from [27]

$$C = \frac{n_1}{S}[1 - \exp(-St_1)]. \quad [31]$$

Substituting $h(z)$ and $g(z)$ in [30] and performing the integration the general solution reduces to

$$n(z, S) = C\frac{m(0)}{m(z)}\exp[-Sa(z)] + \frac{\exp[-Sa(z)]}{m(z)} \cdot \int_0^z \exp[Sa(z')]m(z')[h(z')n(z', 0)]\,dz',\ z > 0 \quad [32]$$

where

$$a(z) = \int_0^z h(z')\,dz' \quad [32a]$$

and

$$m(z) = A(z)u_G(z) \quad [32b]$$

The inversion of the first term yields

$$n_1(z, t) = n_1\frac{m(0)}{m(z)}\{U[t - a(z)] - U[t - (t_1 + a(z))]\}. \quad [33]$$

This term describes the growth of the vapor bubbles introduced at the entrance as they flow along the channel. Equation [33] represents a positive pulse of magnitude $n_1m(0)/m(z)$ and of duration $a(z) < t < (t_1 + a(z))$. Due to the term $a(z)$ this part of the solution accounts for bubble growth due to heat conduction and pressure change.

The inversion of the second term on the right hand side of [32] is conducted formally. Assuming that the Laplace inversion integral can be interchanged with respect to the z' integral we have

$$n_2(z, t) = \int_0^z \frac{m(z')}{m(z)}h(z')n(z', 0)\mathcal{L}^{-1}\{\exp[-S(a(z) - a(z'))]\}\,dz' \quad [34]$$

where $\mathcal{L}^{-1}$ represents the inverse Laplace transformation operator. Now consider

$$\mathcal{L}^{-1}\{\exp[-S(a(z) - a(z'))]\} = \mathcal{L}^{-1}\left\{S\frac{\exp[-S(a(z) - a(z'))]}{S}\right\} = \frac{d}{dt}U[t - (a(z) - a(z'))] = \delta[t - (a(z) - a(z'))]. \quad [35]$$

Hence by [32a] $h(z')\,dz' = da(z')$ we obtain

$$n_2(z, t) = \int_0^{a(z)} \frac{m(z')}{m(z)}n(z', 0)\delta[t - (a(z) - a(z'))]\,da(z'). \quad [36]$$

Equation [36] can be written as

$$n_2(z,t)=\begin{cases}\dfrac{m(z')}{m(z)}\,n(z',0), & 0<t<a(z)\\ 0, & t>a(z)\end{cases} \qquad [37]$$

where z', is the point at which the vapor bubble was originated. z' is given by the explicit solution of

$$a(z')=a(z)-t. \qquad [38]$$

Equations [37] and [38] describe the growth of a vapor nuclei originated at z' as it moves to position z. The complete solution of the vapor phase equation in the general case of the two phase entrance conditions is then given by:

$$n(z,t)=n_1(z,t)+n_2(z,t). \qquad [39]$$

Equation [39] is illustrated for certain parameter values in figure 1. The bubble size function, t, is plotted vs distance from the entrance of the flow channel for the general case of two-phase entrance conditions with $\tau_0=0$ and $P(0)=P_0$. Bubbles of maximum radius corresponding to t_1 exist at the entrance. As the bubbles move along the flow channel their radii increase. In addition, new bubbles of a radius corresponding to $t=0$ are continuously introduced along the channel. The solution has therefore two discontinuities as can be seen from [33] and [37]. The first, at $t_1+a(z)$, corresponds to the maximum radius the bubbles can attain at a certain distance along the channel. At larger radius the bubble number density drops to zero as seen from [33]. The second discontinuity, at $t=a(z)$, represents the boundary between the bubbles introduced at the entrance with density n_1 and the new bubbles which result from growth of vapor nuclei along the channel with density n_2. It is interesting to note that in the case of subcooled or saturated stagnation conditions no bubbles are introduced at the entrance and therefore the group n_1 does not exist.

Equation [39] is used to determine the evaporation rate along the flow channel. From [12],

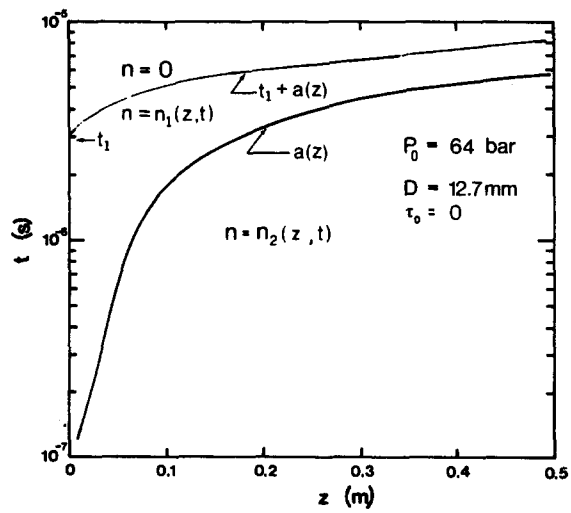

Fig. 1. Variation of bubble size function, t, along a flow path. Curves represent discontinuities between different bubble populations.

[13] and [17] one obtains

$$\Gamma_G = -\frac{4}{3}\pi\rho_G A\beta^2(T_L - T_s)^2 \int_0^{R_\infty} \left(\frac{\partial n}{\partial r}\right) r^3 \, dr. \qquad [40]$$

Equation [40] can be written in terms of τ as:

$$\Gamma_G = -\frac{8\sqrt{2}}{3}\pi\rho_G A\phi(z)(\beta T_s)^5 \int_0^{\tau_\infty} \left(\frac{\partial n}{\partial \tau}\right) \tau^{3/2}. \qquad [41]$$

Since, as shown in figure 1, $n = 0$ at $\tau = \tau_\infty$, [41] can be integrated by part to yield:

$$\Gamma_G = \frac{3}{2} F(z) \int_0^{\tau_\infty} n\tau^{1/2} \, d\tau \qquad [42]$$

where

$$F(z) = \frac{8\sqrt{2}}{3}\pi\rho_G A\phi(z)(\beta T_s)^5.$$

Substituting [39] for $n(z, t)$ in [42] we obtain after some rearrangements:

$$\Gamma_G = \frac{F(z)}{m(z)}\left\{\frac{3}{2}\int_{\tau_0}^{\tau_0 + a(z)} n(z', \tau_0) m(z') \tau^{1/2} \, d\tau + n_1 m(0)[(\tau_1 + a(z))^{3/2} - (\tau_0 + a(z))^{3/2}]\right\}. \qquad [43]$$

Considering the functional relation between τ and z' [38], the integral in [43] can be written in terms of z' as

$$\Gamma_G(z) = \frac{F(z)}{m(z)}\left\{\frac{3}{2}\int_z^0 n(z', \tau_0) m(z')[\tau_0 + a(z) - a(z')]^{1/2} h(z') \, dz' + n_1 m(0)[(\tau_1 + a(z))^{3/2} - (\tau_0 + a(z))^{3/2}]\right\} \qquad [44]$$

Once the pressure and liquid temperature are calculated for $z' < z$ one can determine $n(z', \tau_0)$ from [27], $a(z')$ and $m(z')$ from [32a] and [32b] and perform the integration in [44] to obtain the vapor generation rate at z, $\Gamma_G(z)$. This, in turn, can be substituted into the macroscopic vapor equation [4] to yield, with help of [1]–[3], the pressure and liquid temperature at z.

For subcooled flow the integrand in [44] is zero for the subcooled portion of the expansion for which $T_L < T_s$, The integral term in [44] accounts for the formation and growth of bubbles along the flow path. To apply [44] requires suitable specification of n_0, n_1, ψ and τ_0 in [27]. In the absence of direct measurements of these parameters the assumption is made that $n_0 = n_1$ and $\tau_0 = 0$. This leaves two adjustable parameters in the model, n_0 and ψ which entered the analysis through [24].

It should be noted that since u_G depends on α (and therefore on n), [16] and [26] are non-linear partial differential equations. To apply the solution scheme outlined above, an iterative technique had to be used to linearize [26]. u_G was taken initially as a constant and then updated by the solution $n(z, t)$ from the previous iteration. Typically convergence to within 0.1% is obtained after two iterations.

5. NUMERICAL CALCULATIONS

The field equations were combined by substituting the conservation of mass equation [1]

into [2]–[4]. The resulting set of equations can be represented in the matrix form

$$By = b \qquad [45]$$

where y is a three component vector

$$y^T = \left(\frac{d\alpha}{dz}, \frac{dP}{dz}, \frac{dh_L}{dz}\right) \qquad [46]$$

and B and b are a 3×3 matrix and three component column vector respectively, described in Appendix A.

A fully explicit finite difference scheme has been formulated to solve [45] which yields the pressure, void fraction and liquid enthalpy (or temperature) in the channel. The vapor generation rate $\Gamma_G(z)$ was updated at each mesh point using [44].

5.1 *Entrance geometry*

Equation [45], describes a one-dimensional flow field in a duct of arbitrary geometry. A detailed description of the actual ducts and entrance nozzles geometries were utilized to integrate the field equations along the flow path starting from the input stagnation conditions. In a constant area section the flow field is straight forwardly represented if we take $dA/dz = 0$. The initial values of P, h_L and α are taken as the stagnation values.

6. RESULTS AND DISCUSSION

The theoretical model was qualified in comparison with available high pressure data on adiabatic critical flow of water at subcooled, saturated or two-phase entry conditions. The phase distribution parameter C_0 was arbitrarily set to 1.1 in all computations. This value of C_0 as well as the model used for V_{Gj} (see [8]) were recommended for equilibrium flow situations (Lahey & Moody 1977). However, since the effect of C_0 on the predictions is generally small this deficiency is considered acceptable.

The predicted critical mass flux depends largely on the degree of thermal non-equilibrium in the system which, in turn, is affected by the number density of nucleation sites and bubbles in the mixture. Edwards (1968) recommended bubble densities in the range of 22×10^{11} to 2×10^{14} per m^3. If, in addition, the initial bubble radius and radius difference are assumed as 10^{-5} m the recommended range of initial normalized bubble number density per unit radius and radius difference becomes 2×10^{21} to $2 \times 10^{24}\ m^{-5}$, respectively.† In this work the value of $n_0 = n_1 = 7.5 \times 10^{23}\ m^{-5}$ was found to fit the data best.

The surface parameter, ψ, depends on many parameters such as pipe surface condition, water purity, pipe surface area to fluid volume, etc. No physical model is currently available to compute this parameter but an estimate can be made from Alamgir & Lienhard's (1981) paper. The surface parameter was taken in this work as $\psi = 10^{-8}$ which fits [11] in Alamgir & Lienhard (1981) at its lower bound. Figure 2 gives an indication on the sensitivity of the predicted pressure along a pipe to variations in n_0 and the surface parameter ψ. Illustrative calculations are presented for flow of an initially saturated water in 6.35 mm diameter pipe at stagnation pressure of 67 bar. It has been shown that the results are relatively insensitive to the value of ψ in the range of $< 10^{-5}$. In addition, it is interesting to note that in case of two-phase entry conditions, the rate of vapor generation is dominated by the growth of the relatively large bubbles (n_1) which exist initially at the entrance and the contribution of the new bubbles (n_0) is generally small.

To predict the critical mass-flux as a function of pipe length, an exit mass flux was postulated. The changing flow conditions were then tracked along the pipe starting from the

†We are grateful to the reviewer for suggesting this range of bubble density.

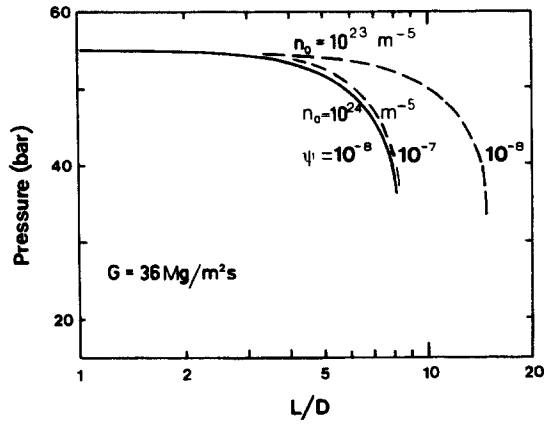

Fig. 2. Effect of n_0 and ψ on the predicted pressure along the flow path.

stagnation point at $z = 0$. At some distance along the pipe the pressure gradient becomes arbitrarily large ($dP/dz > 50$ bar/mm). This point was identified as the choking plane. By repeating the calculations for other mass flow rates one obtains a set of solution points which describes the critical mass flux as a function of pipe length, L.

Critical flow tests were conducted by Sozzi & Sutherland (1975) with saturated, subcooled and boiling water. The effect of initial fluid enthalpy, entrance geometry and flow length was studied. Tests were carried out by blowing down vessels from an initial pressure in the range of 55–75 bar. In figure 3 the present model is compared with data for subcooled and two phase entry conditions. The entrance geometry of nozzle No. 2 in Sozzi & Sutherland (1975) experiments was approximated by a smooth elliptic contour which leads from the vessel into a straight 12.7 mm diameter pipe. The stagnation quality, x_0, indicated in figure 3 is defined by the measured stagnation density. Critical mass fluxes based on a homogeneous equilibrium computations are also indicated in figure 3.

Predictions of the present model are generally shown to be in good agreement with the data. However, critical flow rates in short pipes ($L/D < 2$) are under predicted by 5–10%. This is probably due to the assumption of constant bubble nucleus radius and neglecting the process of bubble nucleation delay at the entrance to the discharge nozzle. Nucleation delay time of about 1 ms has been observed in a number of depressurization tests with water. For subcooled entry conditions a delay of 0.5 ms in bubble generation can shift the choking plane by about 4 cm which is more than three pipe diameters. It should be noted, however, that for two-phase initial conditions, the bubbles at the entrance to the discharge nozzle provide a sufficient number of sites for bulk nucleation that the delay phenomenon is not as pronounced as for subcooled or saturated entry conditions. Very good agreement with the data is therefore obtained for two-phase stagnation conditions with $L/D > 1$.

Fauske (1965) measured the critical flow of initially saturated water in a 6.35 mm diameter pipe over a wide range of stagnation pressure $5 < P_0 < 150$ bar. Horizontal discharge pipes with sharp entrance geometry were used. Test results are compared with model predictions in figure 4. Agreement is shown to be good for long pipes. Critical mass flux is however underpredicted in short pipes ($L/D < 6$). This is probably a result of the inherent limitations of the one dimensional model when applied to describe the physical phenomena in a sharp edged entrance geometry. The predicted rate of bubble growth and formation is sensitive to the pressure conditions and liquid superheat. Therefore, neglecting radial forces in the entrance leads to an erroneous answer due to inaccurate pressure drop prediction. Also, previous investigations (e.g. Edwards 1968) have suggested that an annular flow pattern may exist downstream of a sharp-edged entrance in which a vapor film surrounds a low void fraction two-phase jet. Obviously the bubble growth model does not accurately describe the degree of thermal non-equilibrium in such

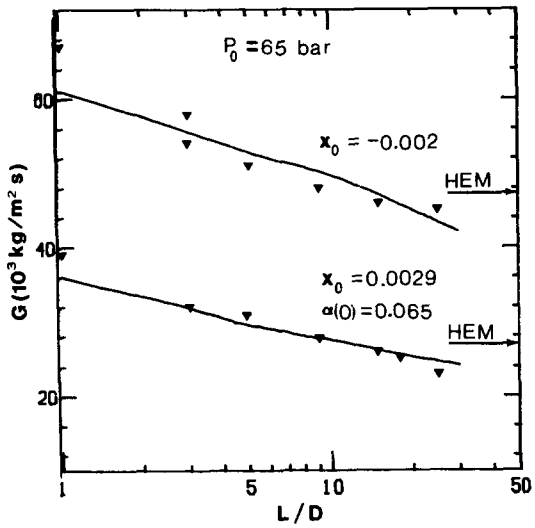

Fig. 3. Comparison of the theoretical predictions with data of Sozzi & Sutherland (1975).

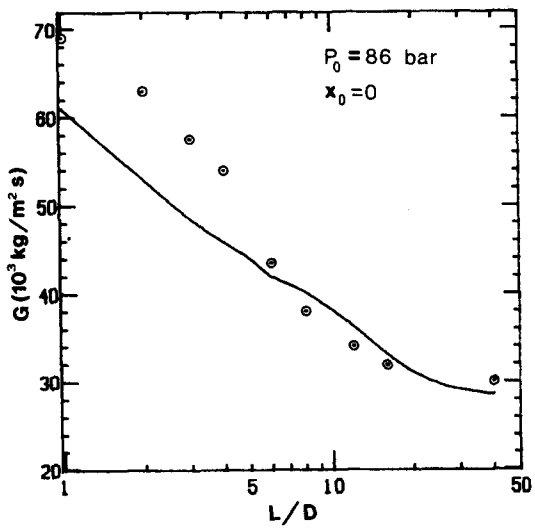

Fig. 4. Comparison of the theoretical predictions with data of Fauske (1965).

separated flow configurations. Increased critical velocity may result from a decreased heat transfer area in annular flow compared to bubbly flow. The entrance effects apparently become small far from the entrance which explains the good agreement between the measured and predicted data for $L/D > 6$.

To investigate the predictive capability of the model for large scale experiments, calculations were performed for a set of blowdown tests of an experimental program made at the Marviken Power Station in Sweden (Abdollahian *et al.* 1982). The discharge nozzle considered for these predictions had a rounded entrance followed by nominally 500 mm constant diameter test section from 166 to 1809 mm in length. Since the upstream conditions changed very slowly during the 50–80 s blowdown, relative to the rapid (100 ms) adjustment of the flow in the test section, the data was treated in a quasi-steady manner, i.e. constant stagnation conditions were assumed. Calculated results are compared with observed mass flow rate for initially subcooled

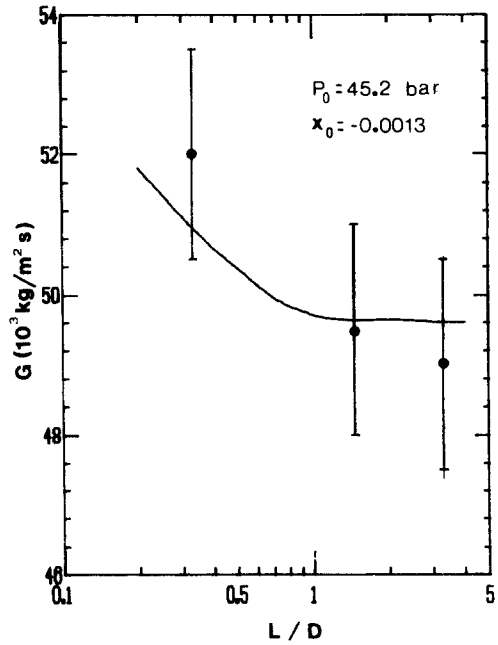

Fig. 5. Comparison of theoretical predictions with Marviken data at subcooled stagnation conditions.

conditions in figure 5. The predicted results agree with the measured flow rate to within the specified measurement accuracy. The experimental data is slightly underpredicted for the short test section. As discussed before, this may be due to bubble nucleation delay.

Data from the Marviken test for initially saturated conditions are compared in figure 6. Good agreement is achieved over the whole range of length. The error bars in figure 6 are those quoted in the experiment.

Flashing water flows in a converging/diverging nozzle were investigated by Abuaf *et al.* (1980). The test section consisted of a symmetrical converging/diverging portion 559 mm long with inside diameter of 51 at the inlet and exit and 25 mm at the throat. Critical flows were measured for inlet water temperature of 99.5°C and inlet pressures in the range of 1–10 bar. Figure 7 compares the predicted and measured inlet critical mass flux as a function of the inlet pressure. The critical inlet mass flux was set so as to induce a choking flow at the nozzle throat. In all cases analyzed inception of flashing ($T_s < T_L$) is also predicted very close to the nozzle throat. These predictions are qualitatively in agreement with the experimental observations. The predicted maximum inlet mass fluxes are also in agreement with the measured data. At the low inlet pressure range the model underpredicts the measured mass flux by 5–10%.

The model was used to compute various parameters of importance for the prediction of two-phase critical flow. For instance, figure 8 shows typical profiles of the vapor and mean velocities and the mixture density along a 6.35 mm diameter horizontal pipe with reservoir pressure of 64 bar. The small vapor drift velocity indicated in figure 8 results from the assumed non-uniform vapor distribution ($C_0 = 1.1$).

Vapor void fraction and velocity ratio profiles for the same run are shown in figure 9. For horizontal pipe with local drift velocity $V_{Gj} = 0$ the velocity ratio is:

$$S = \frac{u_G}{u_L} = \frac{C_0}{1 - \frac{\alpha}{1-\alpha}(C_0 - 1)}. \qquad [47]$$

In figure 9 velocity ratio is 1.175 at a location of one diameter upstream of the choking plane.

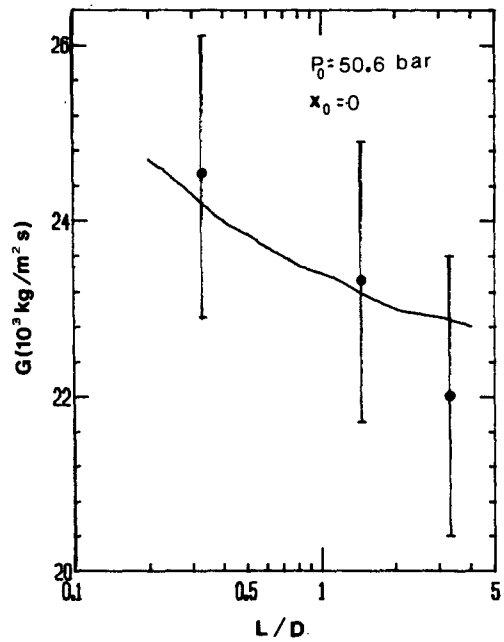

Fig. 6. Comparison of theoretical predictions with Marviken data at saturated stagnation conditions.

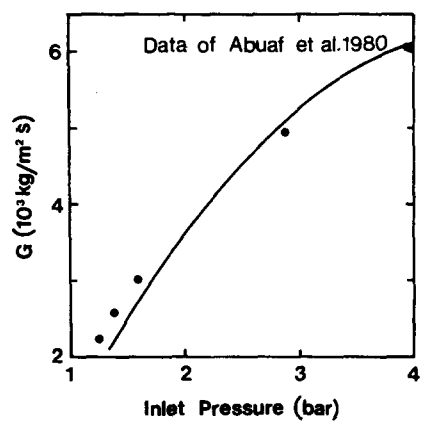

Fig. 7. Comparison of theoretical predictions with experimental data in a converging/diverging nozzle (Abuaf *et al.* 1980).

These relatively small predictions of the interphase relative motion is in general agreement with other theoretical and experimental observations (e.g. Henry *et al.* 1970; Edwards 1968).

Typical profiles of liquid temperature and superheat along the flow channel are shown in figure 10, for Fauske's experimental set-up at stagnation pressure of 86 bar. Liquid temperature is shown to drop by more than 10°K before choking. It should be noted that the liquid temperature is sometimes taken as constant to simplify the analysis (e.g. Ardron 1978). Such an approximation while eliminating the need to solve the energy equation, may lead to erroneous results and overestimation of vapor generation rate. The rate of liquid cooling increases near the choking plane due to rapid depressurization.

Figure 11 shows typical results of Γ_G/A along a 6.35 mm diameter pipe for two mass fluxes and reservoir pressure of 64 bar. The vapor generation rate increases sharply near the choking plant. Γ_G is a function of the stagnation pressure and mass flux.

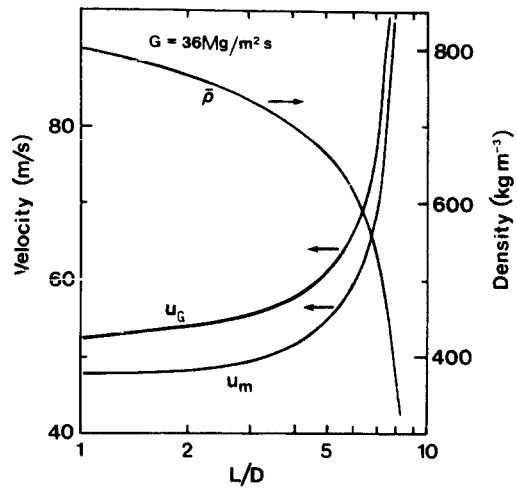

Fig. 8. Typical profiles of mean velocity, u_m, vapor velocity, u_G, and mean density, $\bar{\rho}$, along the flow path.

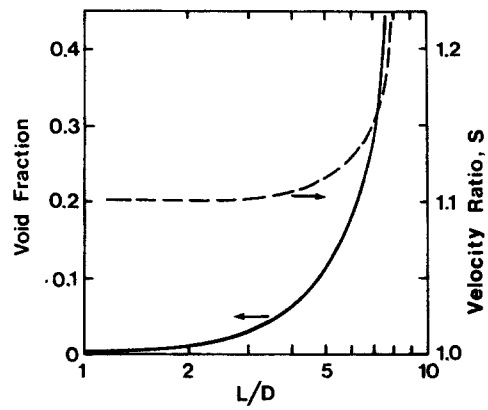

Fig. 9. Void fraction and velocity ratio upstream of the choking plane.

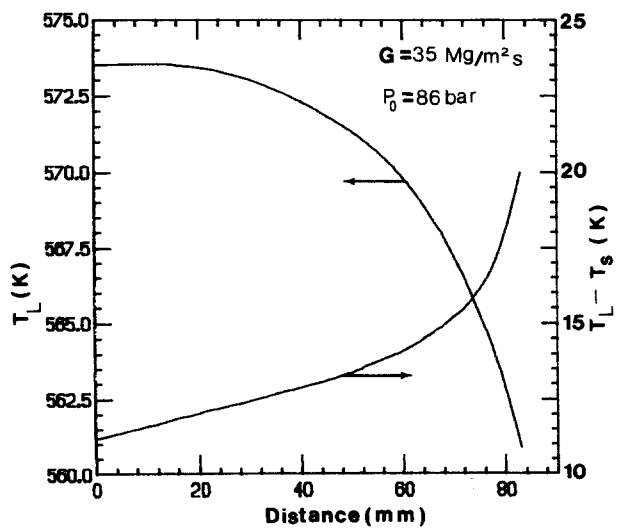

Fig. 10. Variation of liquid temperature and superheat along the flow path.

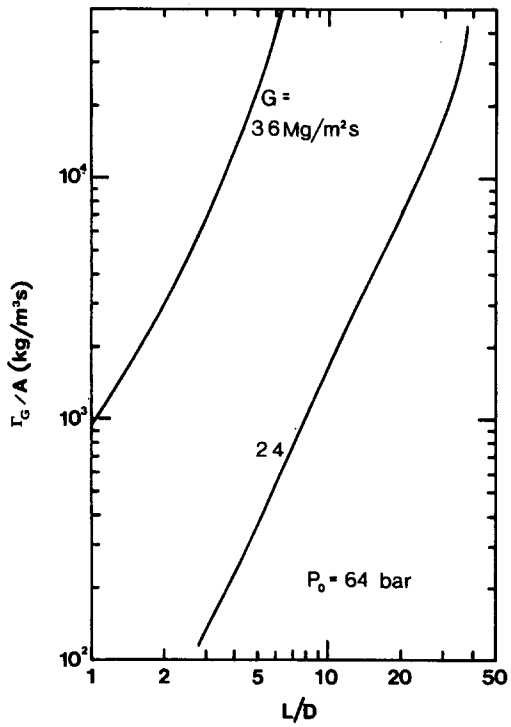

Fig. 11. Typical predictions of vapor generation rate along a pipe.

7. CONCLUSIONS

A one-dimensional, non-equilibrium mechanistic model has been developed to calculate the critical mass flux of an initially two phase, saturated or subcooled liquid discharging from a reservoir. The model is based on the concept of bubble growth being controlled by heat conduction through the surrounding superheated liquid. An approach has been taken to describe the number and size of the vapor bubbles along the flow path which, in turn, determines the linear rate of vaporization. Good agreement with the data over a wide range of stagnation pressures and geometries was obtained by choosing two parameters which describe the initial normalized bubble density and the heterogeneity factor. For all calculations, the empirical constants of the model were unchanged. It is shown that the theory can describe steady state choking phenomena and departure from thermal and mechanical equilibrium.

Limitation of the present theory arises from a single phase entry conditions when applied to very short pipes and high mass fluxes. In these cases the neglect of bubble nucleation delay and flow separation caused a noticeable systematic under prediction of the critical flow rate of subcooled and saturated data. The effect of bubble delay is not pronounced when two-phase entry conditions are analyzed. Mechanistic models for bubble delay, variable nucleus radius and flow separation at the entrance are required for further refinement of the model.

Critical two-phase flow is shown to be a strong function of the size and configuration of the discharge pipe or nozzle. Discharge flow in pipes of up to twenty diameters in length are significantly higher than predicted by a homogeneous thermal equilibrium model. Predictions for long pipes ($L/D > 20$) are affected by flow friction and lie below the predictions based on homogeneous frictionless flow.

Acknowledgements—The authors are indebted to Dr. Sorel Kaizerman for his useful discussions and assistance in formulating the drift flux model, and to Dr. D. Abdollahian for providing many useful suggestions as well as data.

REFERENCES

ABDOLLAHIAN, D., HEALZER, J. & JANSSEN, E. 1980 Critical flow data review and analysis. Part 1: Literature survey. S. Levy, Inc. Report SLI-7908-1.

ABDOLLAHIAN, D., HEALZER, J., JANSSEN, E. & AMOS C. 1982 Critical flow data review and analysis. EPRI NP-2192.

ABUAF, N., WU, B. J. C., ZIMMER, G. A., SAHA, P. & JONES, O. C. Jr. 1980 Non-equilibrium vapor generation rates of flashing water flows. *Proc. ANS/ASME Int. Topical Meeting on Nuclear Reactor Thermal Hydraulics.* Saratoga Springs, New York, pp. 830–841.

ALAMGIR, Md. & LIENHARD, J. H. 1981 Correlation of pressure undershoot during hot-water depressurization. *ASME J. Heat Transfer* **103**, 52–55.

ARDRON, K. H. & FURNESS, R. A. 1976 A study of the critical flow models used in reactor blowdown analysis. *Nucl. Engng Design* **39**, 257–266.

ARDRON, K. H. 1978 A two-fluid model for critical vapor–liquid flow. *Int. J. Multiphase Flow* **4**, 323–337.

BOURE, J. A. 1977 The critical flow phenomenon with reference to two-phase flow and nuclear reactor systems. *ASME Symp. on the Thermal and Hydraulic Aspects of Nuclear Reactor Safety* **1**, 195–216.

CHA, Y. S. & HENRY R. E. 1981 Bubble growth during decompression of liquid, *ASME J. Heat Transfer* **103**, 56–60.

COLE, R. 1979 *Homogeneous and Heterogeneous Nucleation in Boiling Phenomena* (Edited by STRALEN, S. V. & COLE, R.). McGraw Hill, New York.

DOBRAN, F. 1981 On the consistency conditions of averaging operators in 2-phase flow models and on the formulation of magnetohydrodynamic 2-phase flow, *Int. J. Engng Sci.* **19**, 1353–1368.

EDWARDS, A. R. 1968 Conduction controlled flashing of a fluid and the prediction of critical flow rates in a one-dimensional system. UKAEA, Health and Safety Branch, AHSB(S) R 147.

FAUSKE, H. K. 1965 The discharge of saturated water through tubes. *Chem. Engng Prog. Symp. Ser.* **61**, 211–216.

FORSTER, H. K. & ZUBER, N. 1954 Growth of a vapor bubble in a superheated liquid. *J. Appl. Phys.* **25**, 474–478.

HENRY, R. E. 1970 The two-phase critical discharge of initially saturated or subcooled liquid. *Nucl. Sci. Engng* **41**, 336–3421.

HENRY, R. E., FAUSKE, H. K. & MCCOMAS, S. T. 1962 Two-phase critical flow at low qualities—II. Analysis. *Nucl. Sci. Engng* **41**, 92–98.

JONES, O. C. & SAHA, P. 1977 Non equilibrium aspects of water reactor safety. BNL-NUREG 23143.

JONES, O. C. & ZUBER, N. 1978 Bubble growth in variable pressure fields, *ASME J. Heat Transfer* **100**, 453–459.

LAHEY, Jr., R. T. & MOODY, F. J. 1977 *The Thermal Hydraulics of a Boiling Water Reactor,* Chap. 5, American Nuclear Society.

MALNES, D. 1975 *Critical Two-phase Flow Based on Non-equilibrium Effects, Non-Equilibrium Two-Phase Flows* (Edited by LAHEY, R. T. & WALLIS, G. B.) *Am. Soc. Mech. Engrs,* pp. 11–17.

PLESSET, M. S. & ZWICK, S. A. 1954 The growth of vapor bubbles in superheated liquid. *J. Appl. Phys.* **25**, 493–500.

SIMPSON, H. C. & SILVER, R. S. 1962 Theory of one-dimensional, two-phase homogeneous non-equilibrium flow. *Proc. I. Mech. Engng Symp, on Two-Phase Flow,* 45–56.

SOZZI, G. L. & SUTHERLAND, W. A. 1975 Critical flow of saturated and subcooled water at high pressures. G. E. Report HW-13418.

STREETER, V. L. 1961 (Ed.) *Handbook of Fluid Dynamics,* Vol. 3, pp. 16. McGraw-Hill, New York.

WALLIS, G. B. 1980 Critical two-phase flow, *Int. J. Multiphase Flow* **6**, 97–112.

WINTERS, Jr., W. S. & MERTE, Jr., H. 1979 Experiments and non-equilibrium analysis of pipe blowdown, *Nucl. Sci. Engng* **69**, 411–429.

APPENDIX A

To combine the field equations into a matrix form, it is convenient to use the following identities:

$$\bar{\rho} = \alpha\rho_G + (1-\alpha)\rho_L \qquad [A1]$$

$$\bar{\rho}H = \alpha\rho_G + (1-\alpha)\rho_L h_L. \qquad [A2]$$

It is further assumed that V_{Gj}, h_G and ρ_L are sectionally constant and are uniform over the cross-section. With these assumption and using [9] the components of the square matrix B and column vector b in [45] are:

$$B = \begin{bmatrix} B_{11} & B_{12} & 0 \\ B_{21} & B_{22} & B_{23} \\ B_{31} & B_{32} & 0 \end{bmatrix} \qquad [A3]$$

$$B_{11} = \frac{s^2\rho_G}{(1-\alpha)^2\rho_L} + \frac{(\rho_L - \rho_G)\xi}{\bar{\rho}}$$

$$B_{12} = \frac{\bar{\rho}}{G^2} - \left\{\alpha\xi\left[\frac{1}{\rho_G} - \frac{(1-\alpha)(\rho_L-\rho_G)}{\bar{\rho}\rho_G}\right] - \frac{\alpha s^2}{(1-\alpha)\rho_L}\right\}\frac{\mathrm{d}\rho_G}{\mathrm{d}P}$$

$$B_{21} = \frac{\rho_L\rho_G}{\bar{\rho}^2}(1+s) + \gamma(\rho_L - \rho_G)$$

$$B_{22} = \chi - \left[\alpha\gamma - \frac{\alpha(1-\alpha)(1+s)\rho_L}{\bar{\rho}^2}\right]\frac{\mathrm{d}\rho_G}{\mathrm{d}P}$$

$$B_{23} = \frac{1}{h_{LG}\bar{\rho}}[(1-\alpha)\rho_L - s\alpha\rho_G]$$

$$B_{31} = \frac{\rho_L\rho_G}{\bar{\rho}}\mathrm{Eu}_G$$

$$B_{32} = \frac{\rho_L}{\bar{\rho}}E(1-\alpha C_o)\alpha u_G\frac{\mathrm{d}\rho_G}{\mathrm{d}P}$$

where

$$E = \frac{1}{C_0 - (C_0-1)\dfrac{\rho_L}{\bar{\rho}}}$$

$$\gamma = \alpha\rho_G\rho_L\frac{E^2(C_0-1)}{\bar{\rho}^3}\left(C_0 + \frac{\rho_L V_{Gj}}{G}\right)$$

$$\chi = -\frac{1}{h_{LG}\bar{\rho}}\left[1 + \alpha\frac{V'_{Gj}}{G}(\rho_L - \rho_G)\right]$$

$$s = \frac{\rho_L V'_{Gj}}{G}$$

$$\xi = 1 - \frac{\alpha\rho_G s}{\rho_L(1-\alpha)}\left[s - 2sEC_0 - 2E(C_0-1)\frac{\rho_L}{\bar{\rho}}\right].$$

The vector b is

$$b = \begin{bmatrix} b_1 \\ b_2 \\ b_3 \end{bmatrix} \qquad [A4]$$

$$b_1 = \frac{\epsilon}{A}\frac{dA}{dz} - \frac{2f}{D} - \frac{g\bar{\rho}^2 \cos\theta'}{G^2} - \frac{\bar{\rho}}{G^2}\left(\frac{dP}{dz}\right)_{loc.}$$

$$b_2 = \frac{q'' P_H}{GAh_{LG}} - \frac{\alpha\rho_G\rho_L V_{Gj} E}{AG\bar{\rho}}\frac{dA}{dz}$$

$$b_3 = \frac{\Gamma_G}{A} - \frac{1}{A}\left[\alpha u_G \rho_G - \frac{E}{\bar{\rho}}\alpha G C_0 \rho_G\right]\frac{dA}{dz}$$

$$\epsilon = 1 - sE\rho_G \frac{\alpha}{1-\alpha}\left[\frac{V_{Gj}}{G} - \frac{C_0 - 1}{\bar{\rho}}\right].$$

For homogeneous flow [A3] and [A4] are simplified by using

$$E = C_0 = \xi = 1$$

$$s = \gamma = V'_{Gj} = 0$$

$$u_G = \frac{G}{\bar{\rho}}.$$

The resulting matrix and vector for homogeneous flow are

$$B = \begin{bmatrix} \dfrac{\rho_L - \rho_G}{\bar{\rho}} & \dfrac{\bar{\rho}}{G^2} - \dfrac{\alpha}{\bar{\rho}}\dfrac{d\rho_G}{dP} & 0 \\ \dfrac{\rho_L\rho_G}{\bar{\rho}^2} & -\dfrac{1}{h_{LG}\bar{\rho}} + \dfrac{\alpha(1-\alpha)\rho_L}{\bar{\rho}^2}\dfrac{d\rho_G}{dP} & \dfrac{(1-\alpha)\rho_L}{h_{LG}\bar{\rho}} \\ \dfrac{u_G\rho_G\rho_L}{\bar{\rho}} & \dfrac{\alpha(1-\alpha)U_G\rho L}{\bar{\rho}}\dfrac{d\rho_G}{dP} & 0 \end{bmatrix}$$

and

$$b = \begin{bmatrix} \dfrac{1}{A}\dfrac{dA}{dz} - \dfrac{2f}{D} - \dfrac{g\bar{\rho}^2\cos\theta'}{G^2} - \dfrac{\bar{\rho}}{G^2}\left(\dfrac{dP}{dz}\right)_{loc.} \\ \dfrac{q'' P_H}{GAh_{LG}} \\ \dfrac{\Gamma_G}{A} \end{bmatrix}$$